Int J Adv Manuf Technol (2017) 92:4031–4038
DOI 10.1007/s00170-017-0515-7

ORIGINAL ARTICLE

A low-cost infrared sensing system for monitoring the MIG welding process

Peng Yu[1] · **Guocheng Xu**[1] · **Xiaopeng Gu**[1] · **Guanghao Zhou**[1] · **Yukuo Tian**[1]

Received: 12 November 2016 / Accepted: 2 May 2017 / Published online: 9 May 2017

Abstract In this study, a low-cost infrared sensing system based on the analysis of the surface temperature distribution is proposed for monitoring the perturbations occurring during the aluminum alloy metal inert gas (MIG) welding process. A galvanometer scanner is employed in this real-time infrared sensing system to continually reflect the infrared energy to the point infrared sensor. By controlling the scanning mirror of the galvanometer scanner rotating in a high speed, the infrared energy at different points of the welding seam and the heat-affected zone on the surface of the plate will be continually captured by the point infrared sensor. Different conditions (changes in the welding speed, welding current, and joint gap width) of the welding process have been simulated to perturb the welding process. Three representative geometric defects such as undercut, humping, and lack of fusion were produced to validate our infrared sensing system. Experimental results showed that the sensing system is useful for monitoring perturbations that arise during the welding process and identifying welding defects.

Keywords Infrared sensing · Welding monitoring · Humping · Undercut · Lack of fusion

✉ Xiaopeng Gu
guxp@jlu.edu.cn

[1] Key Laboratory of Automobile Materials of Ministry of Education and Department of Materials Science & Engineering, Jilin University, No. 5988 Renmin Street, Changchun 130025, People's Republic of China

1 Introduction

Nowadays, aluminum and its alloys are extensively manufactured and employed in the aerospace, shipbuilding, national defense, and electronic industries, both to protect the environment and meet the growing need for lightweight construction [1, 2]. In practice, however, a butt weld in thin aluminum alloys is always difficult to weld .On the one hand, the deformations during welding are high due to the high coefficient of thermal expansion of aluminum and aluminum alloys; on the other hand, aluminum alloys have a low melting point and they are difficult to see when they melt since there is no color change.

In a real production environment, numbers of uncontrollable factors like contamination and environmental conditions will perturb the welding process. Unexpected perturbations such as deviation of welding current and voltage, plates with improper welding groove geometry, and insufficient gas protection of weld pool will seriously affect the final result. At present, in order to ensure the safety of their productions, companies usually perform post-weld inspections. Many studies used non-destructive testing (NDT) methods such as radiography, ultrasonic, liquid penetrant, and eddy current to detect internal and surface defects of welds [2–6]. However, non-destructive tests mentioned above are always expensive and time consuming. Therefore, the real-time monitoring of the welding process is required by manufacturing industry for reducing the overall production costs and improving the productivity without sacrificing weld quality.

Arc welding is a process in which a very intense, moving heat source is applied to the workpiece. When structural members are joined by fusion welding, the material of the plates has to be heated to its melting point and then cooled again rapidly [7]. Thus, temperature of a certain

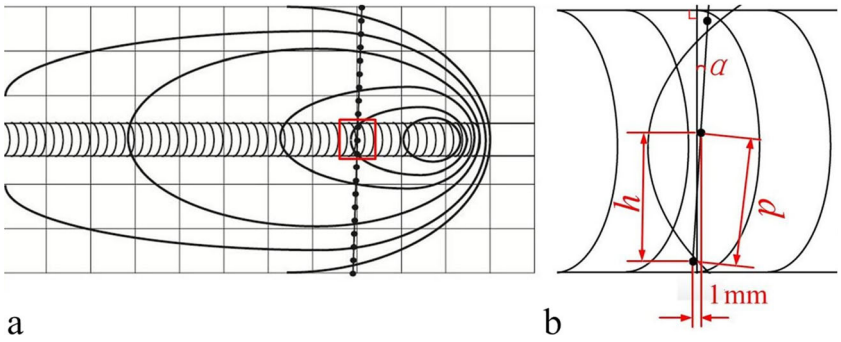

Fig. 1 **a** A line crossed temperature isotherms around moving source when quasi-stationary state is achieved. **b** Magnified image of the *red square*

point on the surface of the plate reaches a maximum value and then cools with time. Except for the initial and final transients of welding, heat flow in a workpiece of sufficient length is quasi-stationary, with respect to the moving heat source. In other words, for an observer moving with the heat source, the surface temperature distribution does not change with time [8].

Arc welding process as mentioned above is inherently a thermal-processing method; thus, infrared sensing is being considered as an effective method for monitoring the welding process. Every object with a temperature above the absolute zero (−273.15 °C = 0 K) emits an electromagnetic radiation from its surface, which is proportional to its intrinsic temperature. A part of this so-called intrinsic radiation is infrared radiation, which can be used to measure a body's temperature. Previous investigations have shown that various disturbances to the welding process will change the heat flow and cause perturbations in the surface temperature distribution which can be picked up by the infrared camera; unique changes in the distribution of temperatures can be taken as reference signals for a particular type of imminent weld defect [9–11].

The surface temperature distribution of the welding pool contains plenty of welding quality information and can reflect the welding stability. To this end, many researches based on the analysis of temperature field of the welding pool and the heat-affected zone have been made to achieve on-line monitoring and controlling of the penetration depth and the bead width [12–17]. Infrared cameras have also been widely applied in real-time monitoring of temperature in gas-shielded fluxcored arc welding (FCAW-G) of steel [18], molten metal filler welding (MMFW) of tin-lead alloy [19], pulsed metal inert gas (P-MIG) welding of low carbon steel [20], and metal inert gas (MIG) welding of steel [21].

However, for a long time, the infrared sensing systems that were mentioned above have not been successfully applied for commercial use; the high initial cost of an area-scan or line-scan infrared camera has been one of main bottlenecks to limit them to be widely used in industry. Furthermore, in some cases, additional large-sized hardware is difficult to embed into manufacturing processes.

A line on the topside plate surface which is perpendicular to the weld is shown in Fig. 1a. It is slightly behind the moving source and crosses isotherms. Temperatures of these points on this line contain plenty of thermal radiation information and have a close relationship with welding quality. In this paper, a low-cost infrared sensing system is utilized for measuring the temperature of points on lines which are approximately perpendicular to the weld in order to monitor the perturbations occurring during the welding process and identify welding defects.

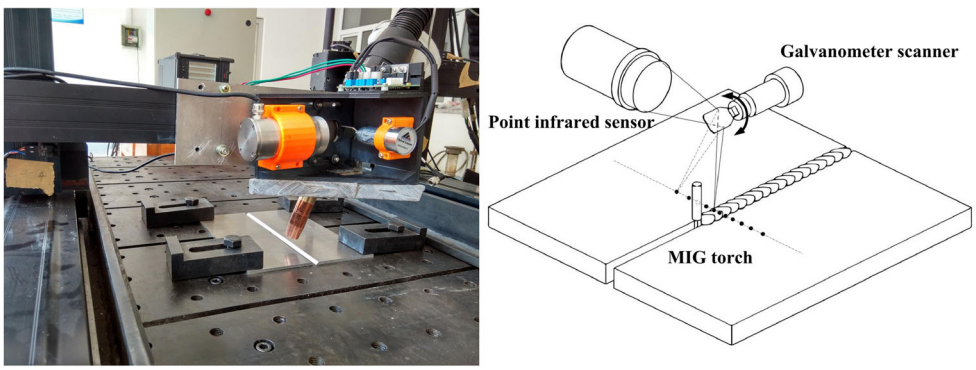

Fig. 2 Experimental setup

Table 1 The position parameters in different welding processes. *d* is the distance between two adjacent points, *h* is the vertical distance between two adjacent points, and α was the deviation angle of the scanning line from perpendicularity

Weld	*v* (mm/s)	α (°)	*h* (mm)	*d* (mm)
Sound	7	89.71	0.07	1.002
Undercut	9	89.53	0.09	1.004
Lack of fusion	10	89.42	0.10	1.005
Humping	14	88.87	0.14	1.010

2 Experimental setup

Figure 2 shows the welding experimental setup that is implemented. The infrared sensing system that is used to obtain the IR radiation from the surface of the plate being welded is made up of a galvanometer scanner and a point infrared sensor. The point infrared sensor is an Optris CTlaser 2MH which is adjusted to a temperature range between 385 and 1600 °C (685.15 to 1873.15 K) with an accuracy of ±1% over the entire range. The exposure time (90%) of the sensor is 1 ms. The software was designed to control the rotational speed and rotation direction of the galvanometer scanner. By controlling the scanning mirror of the galvanometer scanner rotating in a high speed, the infrared energy at different points of the plate being welded will be continually reflected to the point infrared sensor. This made it possible to obtain the temperature distribution of the welding seam and its heat-affected zone by a point infrared sensor. As shown in Fig. 1b, the distance between two measuring points is 1 mm. It costs 10 ms when the scanning mirror of the galvanometer rotates from one position to another and it will hold its position for 5 ms in order to get the average temperature of one point. With the increase of the welding speed, the position parameters will change. The position parameters in different welding processes are listed in Table 1.

The welding generator which is a Fronius Transpuls Synergic 5000 adapted to the Φ 1.2-mm 5087 filler wire metal was chosen. A butt joint welding of 6082–T6 aluminum alloy plates with a thickness of 4 mm, width of 100 mm, and length of 250 mm is tested in the experiments. The plates were brushed with a steel brush to remove oxide layers before positioned and clamped down on the welding table. The chemical composition of the base material and filler wire metal is presented in Table 2. Argon shielding gas was applied with a 15-L min^{-1} flow to protect the weld surface from the effects of the surrounding air. The movements of the welding torch and the infrared sensing system are driven by two sets of servo motors and ball screws. During the MIG welding process, the infrared sensing system keeps a distance (two times the welding speed) with the torch and moves behind the torch at the welding speed. The light fire-resisting brick is set between the welding torch and the infrared sensing system to protect the point infrared sensor from the extensive arc light. The software in this set of experiments is also designed to control the welding speed, to open the arc on the MIG welding process, to control the welding current, and to finish the process. A 10-bit, 20 KS/s multifunction data acquisition board is used to provide integration between the infrared sensing system and the personal computer.

The microhardness across the weld was measured by type MH-3 microhardness tester. Welds were cut and grinded with paper P1000 prior to the hardness measurements. The impression force was set to 100 g and the impression time was 10 s. The hardness measurements were taken from the centerline of the weld beam and out to both sides of the weld with 1-mm distance between the imprints.

3 Results and discussion

3.1 Sensing system response on different welding defects

A first series of aluminum alloy plate welding trials is carried out to obtain the surface temperature distribution when no perturbations are intentionally introduced during the welding process. Figure 3 shows the photograph of a sound weld and the corresponding original temperature signals collected from the whole welding process. Figure 4 shows a weld joint without defects and the temperature profile of a line which crosses the weld beam. It can be seen from the figure that temperature increases from the base material to the weld beam and the curve is almost symmetrical along the centerline of the weld

Table 2 Chemical compositions of base metal and filler wire metal

Al alloy series	Si	Fe	Cu	Mn	Mg	Cr	Zn	Ti	Zr	Al
6082	0.79	0.50	0.10	0.58	0.96	0.25	0.20	0.10	0.00	96.52
5087	0.25	0.40	0.05	0.81	4.60	0.10	0.25	0.15	0.13	93.26

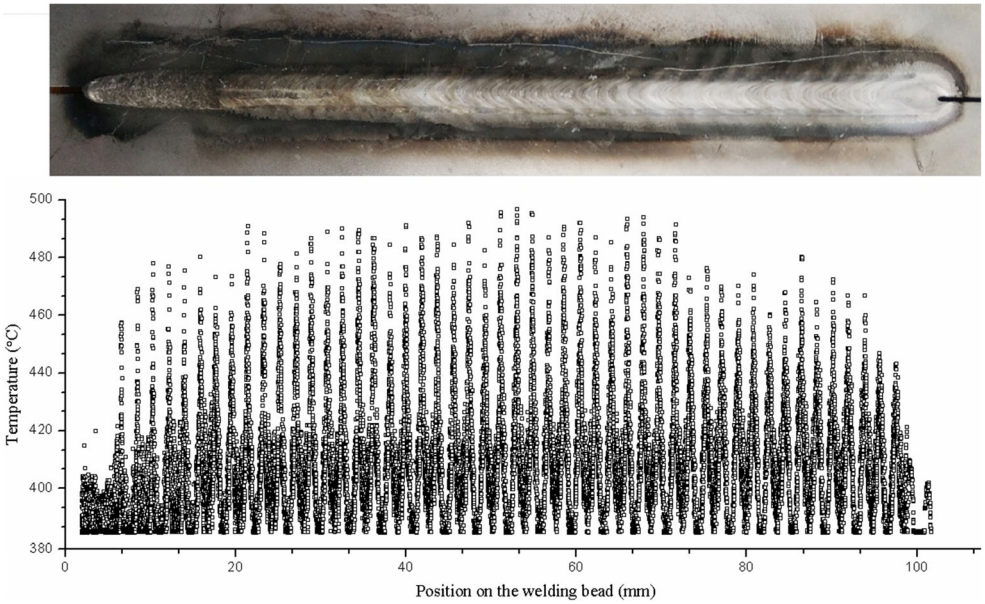

Fig. 3 A sound weld and the corresponding original temperature signals collected from whole welding process

beam. This thermal signature is taken as reference thermal curve for a sound weld.

The temperature profile of a line which crosses the humping area is shown in Fig. 5. In the region

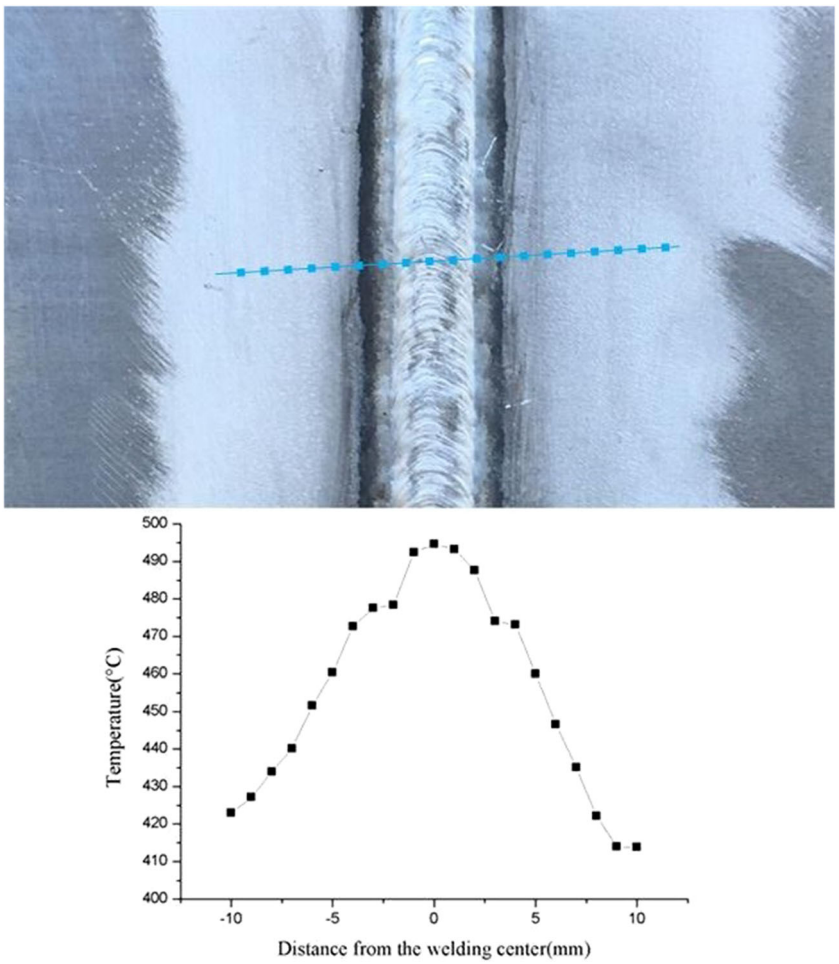

Fig. 4 A sound weld and the temperature profile of a line which crosses the weld beam

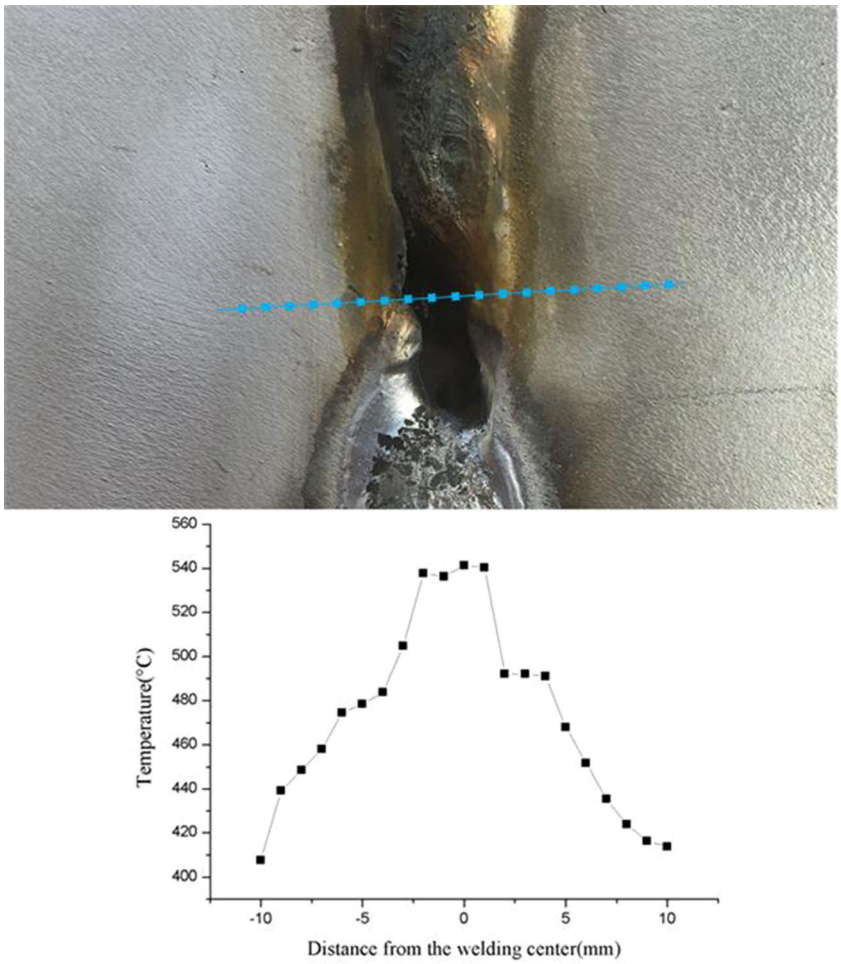

Fig. 5 A weld with humping and the temperature profile of a line which crosses the valley area of the humping

corresponding to the humping defect, the temperature rocketed at the valley area. As there was no weld metal accumulated at this part of the humping, the infrared energy which captured by the infrared sensing system was emitted by the ceramics backing that was set under the plate. The big differences in the typical emissivity between the unoxidized aluminum alloy (0.1–0.2) and the ceramic materials (0.4) resulted in the sharp increase of temperature in this region.

A typical weld flew occurring during high-speed welding process, examined in this experimental session (Fig. 6), is the undercut. The formation of this kind of weld defect is generally due to the improper high welding speed, welding current, or power input during the MIG welding process. Compared with a sound weld, the maximum value of the temperature profile is lower and the temperature went up tardily. The curve is asymmetric, and in particular, at the area adjacent to the undercut, the temperature decrease rapidly. From the authors' point of view, the increase in the welding speed will decrease the welding line energy on the one hand and on the other hand, the heat input in the welding concentrated locally and in terms of time is, in metallic materials, propagated rapidly into more remote areas of the component; such a mechanical notch generated at the weld interface will perturb the heat propagation process.

The last welding defect (lack of fusion) examined in this series of experimental tests is shown in Fig. 7. This kind of defect is relatively common in the mechanical industry and usually caused by the perturbation in the welding current. It is clear from the figure that temperature values at the defect region remain unchanged as there is a little accumulation of weld metal at the lack of fusion area. This thermal signature is taken as reference thermal curve for a welded joint with lack of fusion weld defect.

3.2 Microhardness characterization for temperature validation

The microhardness profile of the sound weld in Fig. 4 is shown in Fig. 8. In the heat-affected zone (HAZ), microhardness drop to the lowest point that is measured in a

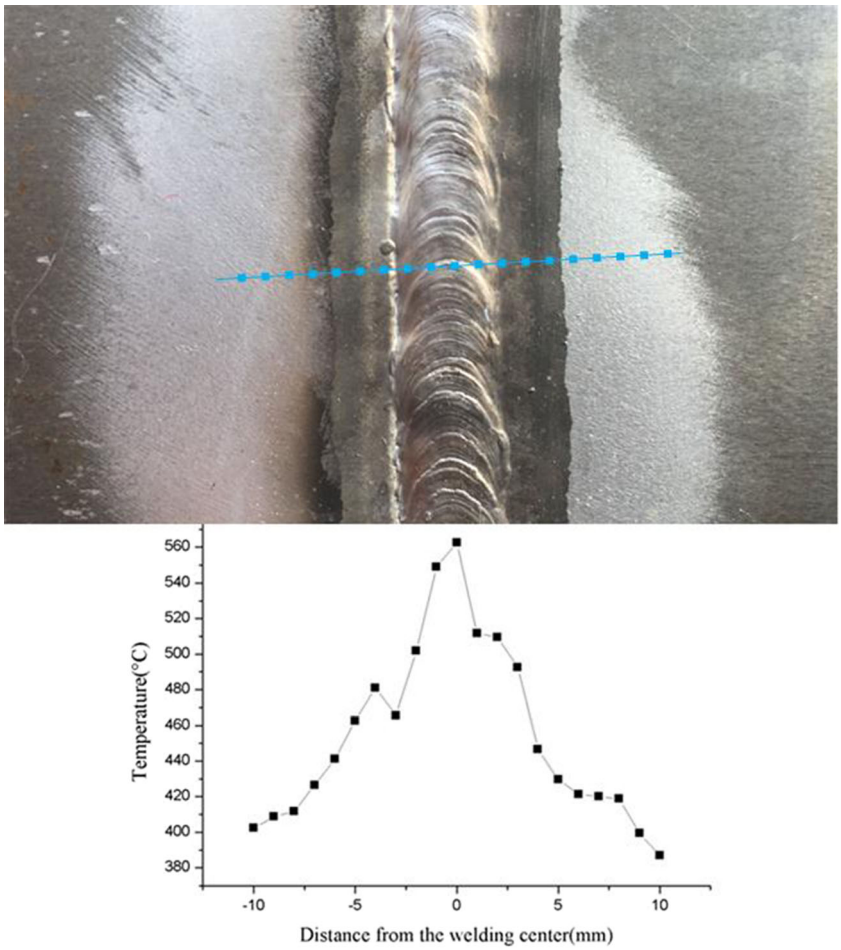

Fig. 6 A weld with undercut and the temperature profile of a line which crosses the weld beam

distance 8 mm from the axis on both sides of the weld where corresponding temperatures are 424.1 and 421.6 °C. Then, the microhardness increases up to 78.4 HV at a distance of 6 mm from the axis on one side of the weld and the maximum value of hardness on the other side is in a distance of 5 mm from the axis of the weld (73.1 HV). Temperatures obtained by the infrared sensing system are 452.3 and 460.2 °C, respectively.

The cooling rates at two different locations (3 and 10 mm from the welding center) of the studied alloy are reported varied from 65 to 20 °C/s, and it is possible to deduce theoretically that the peak temperatures achieved during the heating and cooling thermal cycles increase as distance from the fusion line decreases [22, 23]. The cooling rate at a distance of 8 mm from the axis is 28 °C/s. It increases to 56 and 59 °C/s when the distance varies from 6 to 5 mm.The calculated maximum temperatures of the different positions on the surface of the plate are listed in Table 3.

For the studied aluminum alloy, heating during welding may cause overaging and the formation of precipitates explains the substantial deterioration of HAZ microhardness [22]. The decrease of microhardness is reported to be significant between 220 and 500 °C, due to the reversion of β″-precipitates that will occur to an increasing extent in the peak temperature range from 220 to 500 °C and that is associated with a continuous decrease in the HAZ hardness until the dissolution process is completed [23]. Thus, the maximal reached temperature of the point with the minimal value of hardness is 500 °C This is in good agreement with the value that obtained by the infrared sensing system: 503.9 and 501.4 °C. Furthermore, the maximal reached temperature of hardness in the fusion line is 620 °C (liquidus of the 6082 Al alloy). It matches with the measured temperature in the present study 611.9 and 628.35 °C.

4 Conclusions

A low-cost infrared sensing system based on the analysis of the surface temperature distribution for real-time quality monitoring of MIG welding process and identifying welding defects has been described in this paper. Changes in the welding speed, welding current, and joint gap width were introduced in order to perturb the welding

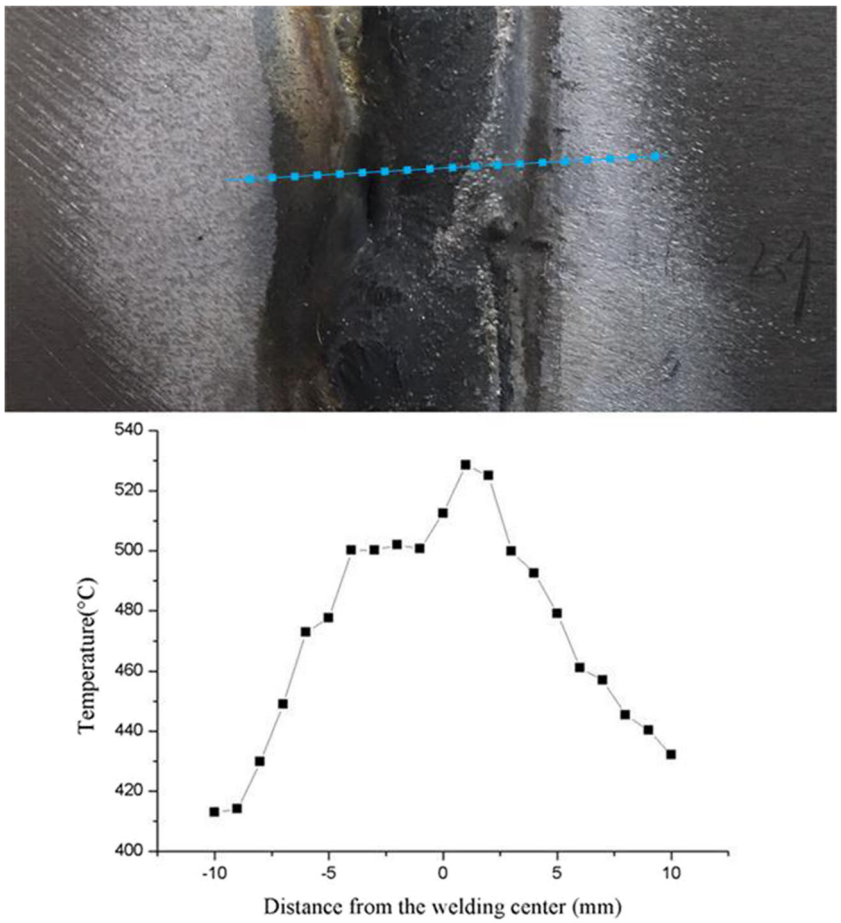

Fig. 7 A weld with lack of fusion and the temperature profile of a line which crosses defect area

process. Three representative geometric defects such as undercut, humping, and lack of fusion were successfully detected. This sensing system is especially attractive for the metal-fabrication industry, due to its small size and low cost that will markedly reduce the overall production costs. Further studies are still needed in order to optimize the device performance in order to steadily collect the temperature in industrial environment. Some important conclusions are listed as follows:

1. The temperature profiles of lines which crosses the weld bead can be used for on-line monitoring of weld quality during MIG welding process of 6082 T-6 aluminum alloy.
2. The formation of defects such as undercut, humping, and lack of fusion will induce unique changes on the temperature field; these changes can be used as reference thermal signals for identifying welding defects
3. The experimental results confirm that IR technique is a sensitive and convenient tool to monitor the presence of weld defects during the welding process.

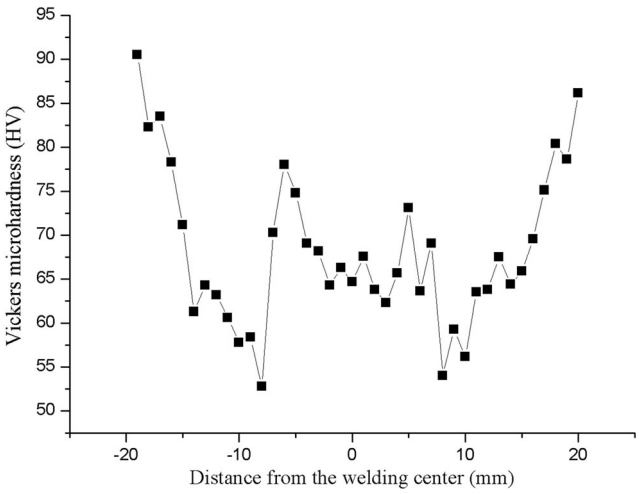

Fig. 8 Microhardness profile of welded joint without defects

Table 3 The calculated maximum temperature of the different positions

Distance from the axis of the weld (mm)	Calculated maximum temperatures (°C)
5 (right)	611.90
6 (left)	628.35
8 (left)	503.90
8 (right)	501.40

References

1. Çam G, İpekoğlu G (2016) Recent developments in joining of aluminum alloys. Int J Adv Manuf Technol. doi:10.1007/s00170-016-9861-0
2. Santos MC Jr, Machado AR, Sales WF, Barrozo MAS, Ezugwu EO (2016) Machining of aluminum alloys: a review. Int J Adv Manuf Technol. doi: 10.1007/s00170-016-8431-9
3. Trimm M (2003) An overview of nondestructive evaluation methods. J Fail Anal Prev 3(3):17–31
4. Lakshmi MRV, Mondal AK, Jadhav CK, Dutta BVR, Sreedhar S (2013) Overview of NDT methods applied on an aero engine turbine rotor blade. Insight Non Destr Test Cond Monit 55(9):482–486. doi:10.1784/insi.2012.55.9.482
5. Lhémery A, Calmon P, Lecœur-Taïbi I, Raillon R, Paradis L (2000) Modeling tools for ultrasonic inspection of welds. NDT E Int 33(7):499–513. doi:10.1016/S0963-8695(00)00021-9
6. Ditchburn RJ, Burke SK, Scala CM (1996) NDT of welds: state of the art. NDT E Int 29(96):111–117. doi:10.1016/0963-8695(96)00010-2
7. Easterling K (1992) Introduction to the physical metallurgy of welding. Butterworth Heinemann, Great Britain
8. Kou S (2003) Welding metallurgy. Wiley, New Jersey
9. Gao X, Liu Y, Lan C, Xiao Z, Chen X (2016) Laser-induced infrared characteristic analysis for evaluating joint deviation during austenitic stainless steel laser welding. Int J Adv Manuf Technol 88(5):1877–1888. doi: 10.1007/s00170-016-8892-x
10. Alfaro SCA, Vargas JAR, Carvalho GCD, Souza GGD (2015) Characterization of "humping" in the GTA welding process using infrared images. J Mater Process Technol 223:216–224. doi:10.1016/j.jmatprotec.2015.03.052
11. Vasudevan M, Chandrasekhar MN, Maduraimuthu MV, Bhaduri AK, Raj B (2013) Real-time monitoring of weld pool during GTAW using infrared thermography and analysis of infrared thermal images. Weld World 55(7–8):83–89
12. Doumanidis CC, Hardt DE (1991) Multivariable adaptive control of thermal properties during welding. J Dyn Syst Meas Control Trans ASME 113(1):82–92
13. Chandrasekhar N, Vasudevan M, Bhaduri AK, Jayakumar T (2015) Intelligent modeling for estimating weld bead width and depth of penetration from infra-red thermal images of the weld pool. J Intell Manuf 26(1):1–13. doi:10.1007/s10845-013-0762-x
14. Menaka M, Vasudevan M, Venkatraman B, Raj B (2005) Estimating bead width and depth of penetration during welding by infrared thermal imaging. Insight Non Destr Test Cond Monit 47(47):564–568. doi:10.1784/insi.2005.47.9.564
15. Ghanty P, Vasudevan M, Mukherjee DP, Pal NR, Chandrasekhar N, Maduraimuthu V, Bhaduri AK, Barat P, Raj B (2008) Artificial neural network approach for estimating weld bead width and depth of penetration from infrared thermal image of weld pool. Sci Technol Weld Join 60(2):395–401. doi:10.1179/174329308X300118
16. Fan H, Ravala NK, Iii HCW, Chin BA (2003) Low-cost infrared sensing system for monitoring the welding process in the presence of plate inclination angle. J Mater Process Technol 140(1–3):668–675. doi:10.1016/S0924-0136(03)00836-7
17. Iii HCW, Kottilingam S, Zee RH, Chin BA (2001) Infrared sensing techniques for penetration depth control of the submerged arc welding process. J Mater Process Technol 113(1–3):228–233. doi:10.1016/S0924-0136(01)00587-8
18. Ling KH, Fuh YK, Kuo TC, Sheng XT (2015) Effect of welding sequence of a multi-pass temper bead in gas-shielded flux-cored arc welding process: hardness, microstructure, and impact toughness analysis. Int J Adv Manuf Technol 81(5):1–14. doi:10.1007/s00170-015-7277-x
19. Wu S, Gao H, Zhang Z (2015) A preliminary test of a novel molten metal filler welding process. Int J Adv Manuf Technol 80(1):647–655. doi:10.1007/s00170-015-7017-2
20. Pal K, Bhattacharya S, Pal SK (2010) Multisensor-based monitoring of weld deposition and plate distortion for various torch angles in pulsed MIG welding. Int J Adv Manuf Technol 50(5):543–556. doi:10.1007/s00170-010-2523-8
21. Al-Habaibeh A, Parkin R (2003) An autonomous low-cost infrared system for the on-line monitoring of manufacturing processes using novelty detection. Int J Adv Manuf Technol 22(3):249–258. doi:10.1007/s00170-002-1467-z
22. Myhr OR, Kluken AO, Klokkehaug S, Fjaer HG, Grong O (1998) Modeling of microstructure evolution, residual stresses and distortions in 6082-t6 aluminum weldments. Weld J 77(7)
23. Missori S, Pezzuti E (2010) Microstructural and mechanical characteristics of welded joints in type 6082-t6 aluminium alloy. Weld Int 11(11):468–474. doi:10.1080/09507119709451996